**DTU Library**

# Reference-free THz-TDS conductivity analysis of thin conducting films

**Whelan, Patrick Rebsdorf; Shen, Qian; Luo, Da; Wang, Meihui; Ruoff, Rodney S.; Jepsen, Peter Uhd; Bøggild, Peter; Zhou, Binbin**

[Link back to DTU Orbit](#)

# Reference-free THz-TDS conductivity analysis of thin conducting films

**PATRICK R. WHELAN,**[1,2,10] **QIAN SHEN,**[3,4,5,10] **DA LUO,**[6] **MEIHUI WANG,**[7] **RODNEY S. RUOFF,**[6,7,8,9] **PETER U. JEPSEN,**[2,3] **PETER BØGGILD,**[1,2,11] **AND BINBIN ZHOU**[3,12]

[1]*DTU Physics, Technical University of Denmark, Ørsteds Plads 345C, 2800 Kongens Lyngby, Denmark*
[2]*Center for Nanostructured Graphene (CNG), Technical University of Denmark, Ørsteds Plads 345C, 2800 Kongens Lyngby, Denmark*
[3]*DTU Fotonik, Technical University of Denmark, Ørsteds Plads 343, 2800 Kongens Lyngby, Denmark*
[4]*School of Information Engineering, Nanchang University, Nanchang 330031, China*
[5]*College of Science, Zhejiang University of Technology, Hangzhou 310014, China*
[6]*Center for Multidimensional Carbon Materials (CMCM), Institute for Basic Science (IBS), Ulsan 44919, South Korea*
[7]*Department of Chemistry, Ulsan National Institute of Science and Technology (UNIST), Ulsan 44919, South Korea*
[8]*School of Materials Science and Engineering, Ulsan National Institute of Science and Technology (UNIST), Ulsan 44919, South Korea*
[9]*School of Energy and Chemical Engineering, Ulsan National Institute of Science and Technology (UNIST), Ulsan 44919, South Korea*
[10]*These authors contributed equally to the work*
[11]*pbog@dtu.dk*
[12]*zhou@fotonik.dtu.dk*

**Abstract:** We present a reference-free method to determine electrical parameters of thin conducting films by steady state transmission-mode terahertz time-domain spectroscopy (THz-TDS). We demonstrate that the frequency-dependent AC conductivity of graphene can be acquired by comparing the directly transmitted THz pulse with a transient internal reflection within the substrate which avoids the need for a standard reference scan. The DC sheet conductivity, scattering time, carrier density, mobility, and Fermi velocity of graphene are retrieved subsequently by fitting the AC conductivity with the Drude model. This reference-free method was investigated with two complementary THz setups: one commercial fibre-coupled THz spectrometer with fast scanning rate (0.2-1.5 THz) and one air-plasma based ultra-broadband THz spectrometer for greatly extended frequency range (2-10 THz). Certain propagation correction terms for more accurate retrieval of electrical parameters are discussed.

## 1. Introduction

Terahertz time-domain spectroscopy (THz-TDS) is maturing as a large-area, fast, accurate and non-invasive measurement technique for extracting the electrical properties of graphene [1–5]. Numerous studies on the applicability of THz-TDS for electrical characterization of graphene exist and conductivity mapping for graphene samples up to $25 \times 30$ cm$^2$ in size have been demonstrated [2,6]. So far, most of the THz-TDS measurements are performed in transmission mode and require two separate scans to determine the electrical properties of graphene: one so-called reference scan recorded through bare supporting substrate and another sample scan through the part of substrate covered by graphene. The reference measurements can essentially single out the graphene interaction with the incident THz waves and lead to accurate retrieval of the electrical properties of graphene. However, it is also highly dependent on the THz-TDS

system exhibiting no signal fluctuations over time (for instance periodic sampling errors [7], timing jitter [8], and uneven mechanical stage movement) in order for the comparison between sample and reference measurement to be solid.

A technique for measuring the conductivity which do not require the standard reference waveform scan is very desirable. This has previously been achieved for reflection-mode THz-TDS on THz transparent substrates, where the THz-TDS waveform contains transients from a directly reflected pulse from the front surface and from reflection at the back surface of the substrate. This technique has been successfully demonstrated on measurements of dielectrics [9,10] and for graphene conductivity [11,12]. In transmission-mode THz-TDS, the recorded waveform similarly consists of a directly transmitted pulse followed by transients from internal reflections (echoes) inside the substrate. These echoes have previously been utilized to improve the retrieval of the conductivity of graphene by comparing the same order of echo signal from reference and sample measurements [8,13,14]. In fact, an echo signal from the sample measurement, when compared with the direct transmitted signal from the same transmission-mode scan, can lead to the retrieval of sample properties without the need for the standard reference scan. Very recently, this type of reference-free methodology has been applied to determine the refractive index and wave impedance of dielectrics [15].

In this study, we extend the methodology to measure the electrical properties of thin conducting films. Especially, two complementary THz setups including a low bandwidth commercial THz-TDS setup capable of spatially mapping samples and another ultra-broadband custom-built system with greatly extended bandwidth are used for detailed investigations. We identify two important correction terms that diminish retrieval errors for the reference-free analysis and demonstrate the extraction of graphene conductivity from the reference-free analysis both with and without inclusion of the correction terms. Furthermore, with the reference-free technique we demonstrate spatial mapping of a wide range of electrical parameters of graphene, such as DC sheet conductivity $\sigma_{DC}$, scattering time $\tau$, carrier density $n$, mobility $\mu$, and renormalized Fermi velocity $v_F^*$.

## 2. Materials and methods

### 2.1. Graphene growth and transfer

Graphene was grown by chemical vapor deposition (CVD) on Cu (111) foils [16] prepared by contact-free annealing [17]. The subsequent transfer to 90 nm $SiO_2$ on high-resistivity Si substrates was performed by bubbling transfer [18].

### 2.2. Optical microscopy

Optical images of graphene were acquired using a Nikon Eclipse L200N microscope equipped with a programmable Prior Scientific stage. Optical maps were generated by stitching together multiple optical images acquired with 20x magnification. Graphene coverage maps were generated by comparing the red, green, and blue (RGB) contrast from each recorded pixel of the optical map to the theoretically calculated contrast for graphene on 90 nm $SiO_2$ substrate [19]. Each pixel in an optical map is then categorized as either substrate (white), single layer graphene (SLG, light gray), bilayer graphene (BLG, dark gray), or other (black), where other contains for instance three (or more) layers of graphene and contaminants/residue from growth and transfer processing [19].

### 2.3. Standard referenced THz-TDS measurements

Two setups were employed for the THz-TDS measurements of graphene - a commercial fiber-coupled spectrometer and a custom-built ultra-broadband THz setup. The commercial system covers a frequency range of ~0.2-1.5 THz and can spatially map the electrical parameters of

graphene by raster scanning samples at normal incidence in the focal plane of the THz beam [14]. The custom-built setup is based on two-color femtosecond air-plasma THz generation and an air biased coherent detection (ABCD) scheme [20–22]. It covers a greatly extended spectral bandwidth of ~2-10 THz for graphene on Si substrate.

The standard referenced THz-TDS measurement is based on the transmission function $\tilde{T}_{\text{film}}(\omega) = \tilde{E}_{\text{film}}(\omega)/\tilde{E}_{\text{sub}}(\omega)$, where $\tilde{E}_{\text{film}}(\omega)$ and $\tilde{E}_{\text{sub}}(\omega)$ are the Fourier transforms of the THz transients transmitted through graphene covered substrate and non-graphene covered substrate, respectively. The incident THz pulse is split into several transients (direct transmission and multiple echo signals) due to internal reflections when passing through the Si substrate as shown in Fig. 1. The transmitted transients are equally separated in time and the separation is determined by the refractive index and thickness of the substrate. When the temporal separation is significant longer than the THz pulse duration, each transient is separate and can be selected by applying a proper window function.
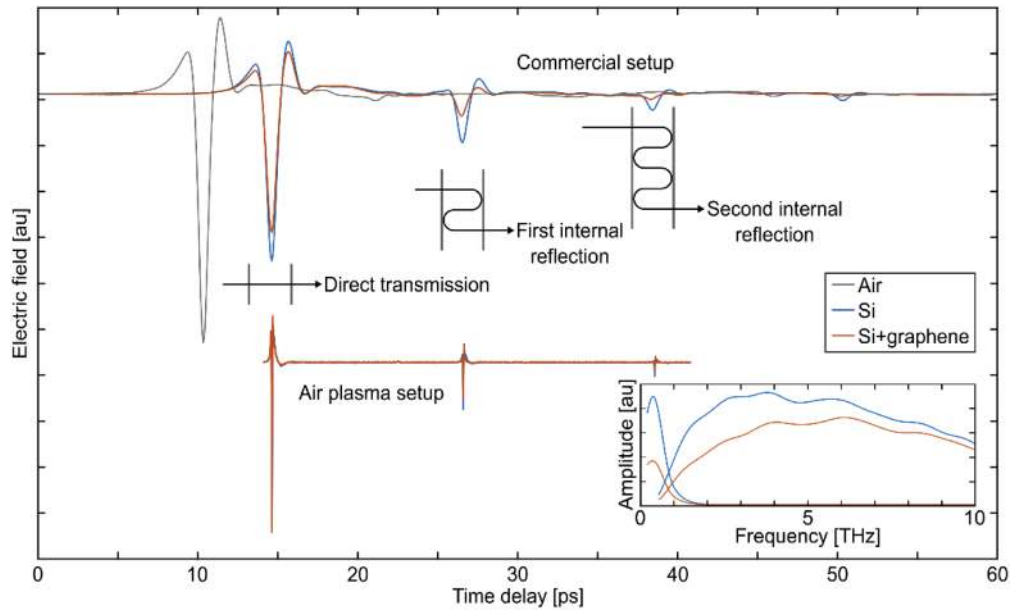


**Fig. 1.** Comparison of time-domain waveforms of THz pulses after transmission through a bare Si substrate and a graphene covered substrate with custom-built broadband or commercial THz spectrometer. The transients originating from internal reflections within the substrate are highlighted. Inset shows Fourier transform of the transients from the first internal reflection for both setups.

The standard referenced analysis in this work is based on the first echo transmission signal (with two internal reflections, or three single-pass inside the substrate). In this case the transmission function

$$\tilde{T}_{\text{film}}^{(1st)} = \frac{\tilde{E}_{\text{film}}^{(1st)}}{\tilde{E}_{\text{sub}}^{(1st)}} = \frac{E_0 \tilde{t}_{\text{film}} \tilde{r}_{\text{sub,air}} \tilde{r}_{\text{film}} \tilde{t}_{\text{sub,air}} \tilde{p}_3}{E_0 \tilde{t}_{\text{air,sub}} \tilde{r}_{\text{sub, air}}^2 \tilde{t}_{\text{sub, air}} \tilde{p}_3} = \frac{\tilde{t}_{\text{film}} \tilde{r}_{\text{film}}}{\tilde{t}_{\text{air, sub}} \tilde{r}_{\text{sub, air}}}, \tag{1}$$

where $\tilde{E}_{\text{film}}^{(1st)}$ and $\tilde{E}_{\text{sub}}^{(1st)}$ is the Fourier transform of first echo signal through the graphene covered substrate and bare substrate, respectively; $\tilde{p}_3$ represents the propagation term in the substrate after three single-passes as the first echo transmission signal experiences. The single-pass propagation term in a substrate with refractive index $\tilde{n}_{\text{sub}}$ and thickness $d_{\text{sub}}$ reads $\tilde{p}_1 = e^{-i\omega d_{\text{sub}} \tilde{n}_{\text{sub}}/c}$. The transmission and reflection coefficients between substrate and air ($\tilde{t}_{\text{air,sub}}$, $\tilde{r}_{\text{sub,air}}$) are calculated

from the Fresnel equations. For $d_{\text{film}} << \lambda/n_{\text{film}}$, the influence of a conducting film is described by the Tinkham equation; the transmission coefficient from air to substrate through a thin conducting film and the reflection coefficient from substrate to air through a thin conducting film are determined as $\tilde{t}_{\text{film}} = 2/(\tilde{n}_{\text{sub}} + 1 + Z_0\tilde{\sigma}_s(\omega))$ and $\tilde{r}_{\text{film}} = (\tilde{n}_{\text{sub}}-1-Z_0\tilde{\sigma}_s(\omega))/(\tilde{n}_{\text{sub}}+1+Z_0\tilde{\sigma}_s(\omega))$ [23], where $Z_0$ is the vacuum impedance. The frequency-dependent sheet conductivity of graphene $\tilde{\sigma}_s^{\text{1st}}(\omega) = \sigma_1+i\sigma_2$ is then [2,8]

$$\tilde{\sigma}_s^{(1\text{st})}(\omega) = \frac{n_A\sqrt{n_A^2 + 4n_An_B\tilde{T}_{\text{film}}^{(1\text{st})}(\omega) + 4n_B^2\tilde{T}_{\text{film}}^{(1\text{st})}(\omega)} - n_A^2 - 2n_An_B\tilde{T}_{\text{film}}^{(1\text{st})}(\omega)}{2n_BZ_0\tilde{T}_{\text{film}}^{(1\text{st})}(\omega)}, \tag{2}$$

where $n_A = \tilde{n}_{\text{sub}}+1$, $n_B = \tilde{n}_{\text{sub}}-1$. It is possible to extract $\sigma_{\text{DC}}$ and $\tau$ in each measurement point by fitting with the Drude model $\tilde{\sigma}_s(\omega) = \sigma_{\text{DC}}/(1 - i\omega\tau)$ [2,6,24,25]. Following semi-classical Boltzmann transport theory [2,26], the calculation of $n$ and $\mu$ from $\sigma_{\text{DC}}$ and $\tau$ follows as [24,25,27]

$$n = \frac{\pi\hbar^2}{e^4v_F^2}\left(\frac{\sigma_{\text{DC}}}{\tau}\right)^2, \tag{3}$$

$$\mu = \frac{e^3v_F^2}{\pi\hbar^2}\frac{\tau^2}{\sigma_{\text{DC}}}, \tag{4}$$

where $v_F$ is the Fermi velocity. It is necessary to renormalize $v_F$ ($v_F^*$) due to interacting electrons in graphene [28–30]. This renormalization is essential for accurate determination of carrier density $n$ and mobility $\mu$ from THz-TDS measurements [27] and is performed by determining $v_F^*$ as $v_F^*/v_F = 1 + C(\alpha)\alpha \ln(\Lambda/k_F)$, where $\Lambda = 1.75$ Å$^{-1}$, $k_F = \sqrt{\pi n}$, $C(\alpha) = (4(1+(\pi/2)\alpha))^{-1}$ and $\alpha = e^2/(4\pi\hbar v_F\varepsilon\varepsilon_0)$ [30].

## 2.4. Self-referenced THz-TDS measurements

Instead of using a THz-TDS reference measurement of a bare substrate for extracting $\tilde{\sigma}_s(\omega)$ as described in Eq. (1), we here show how this can be achieved from a single measurement of graphene covered substrate by comparing the transient from the first echo with the directly transmitted pulse. A transmission function for the ratio of the transients from the first echo relative to the directly transmitted pulse can be written as:

$$\tilde{T}_{\text{film}}^{(\text{ref - free})} = \frac{\tilde{E}_{\text{film}}^{(1\text{st})}}{\tilde{E}_{\text{film}}^{(\text{dir})}} = \frac{E_0\tilde{t}_{\text{film}}\tilde{r}_{\text{sub,air}}\tilde{r}_{\text{film}}\tilde{t}_{\text{sub,air}}\tilde{p}_3}{E_0\tilde{t}_{\text{film}}\tilde{t}_{\text{sub,air}}\tilde{p}_1} = \tilde{r}_{\text{sub,air}}\tilde{r}_{\text{film}}\Delta\tilde{p}. \tag{5}$$

where $\tilde{E}_{\text{film}}^{(\text{dir})}$ is the Fourier transform of directly transmitted pulse through the graphene covered substrate and $\Delta\tilde{p}$ is the propagation factor difference between single pass through the substrate and one additional round-trip inside the substrate. Using $\tilde{r}_{\text{film}} = (n_{\text{sub}} - 1 - Z_0\tilde{\sigma}_s(\omega))/(n_{\text{sub}}+1+Z_0\tilde{\sigma}_s(\omega))$ it is then possible to calculate $\tilde{\sigma}_s^{(\text{ref - free})}(\omega)$ as

$$\tilde{\sigma}_s^{(\text{ref - free})}(\omega) = \frac{n_B^2\Delta\tilde{p} - n_A^2\tilde{T}_{\text{film}}^{(\text{ref - free})}(\omega)}{Z_0(n_A\tilde{T}_{\text{film}}^{(\text{ref - free})}(\omega) + n_B\Delta\tilde{p})}. \tag{6}$$

The transmission function $\tilde{T}_{\text{film}}^{(\text{ref - free})}$ can be obtained from the Fourier transform of the time-windowed transients of the directly transmitted pulse and the first internal reflection. However, unlike Eqs. (1) and 2 for standard referenced analysis, where all the THz wave propagation factors through the substrate are cancelled out in the paired reference-sample measurements, the successful extraction of graphene conductivity by this reference-free method relies on the determination of the differential propagation term $\Delta\tilde{p}$ from the substrate material.

Generally, $\Delta\tilde{p} = \tilde{p}_3/\tilde{p}_1 = e^{-2i\omega d_{sub}n_{sub}/c}e^{-i\emptyset_G}e^{d_{sub}\alpha}$. The first term is a phase term due to the additional round trip propagation inside the substrate, which, in the ideal case, is the only significant term. The second term is a phase correction term where $\emptyset_G$ represents the Gouy phase shift. In reality, when comparing the first echo with the directly transmission pulse, we would expect a certain Gouy phase shift from the additional round-trip propagation of the focused THz beam. The necessity of the Gouy phase shift correction for accurate THz-TDS retrieval has been reported, especially at low THz frequency range (below 1.5 THz) [31]. The last term is an amplitude correction term with $\alpha$ as the frequency-dependent absorption coefficient of the substrate. For well-known substrate materials, the value of $n_{sub}$ is readily available and $d_{sub}$ can be measured beforehand, or accurately determined from the same multi-echo waveform measurement. In this study, a well-characterized high-resistivity Si substrate is chosen, which has a nearly constant ($n_{sub} = 3.417$) real refractive index and high transparency across a broadband THz range [32]. We will discuss further details about the correction terms and the implementation of the reference-free analysis with or without including correction terms with two complementary THz-TDS systems. We use the electrical properties of graphene extracted from standard referenced analysis to compare and validate the extracted values from the reference-free analysis.

## 3. Results and discussions

Time-domain waveforms of a THz pulse after transmission through a sample from the two different setups are shown in Fig. 1. The acquired time-domain waveforms contain several transients originating from internal reflections in the substrate. The first transient from the directly transmitted part of the original incident THz pulse has the largest amplitude with the signal strength decreasing for the following transients.

The transmission function $\tilde{T}_{film}^{(ref\text{-}free)}$ for the reference-free analysis can be easily obtained from the directly transmitted and the first echo transients following Eq. (5). For the differential propagation term $\Delta\tilde{p}$, $n_{sub} = 3.417$ from low frequency up to 15 THz. We determine $d_{sub}$ based on the Fourier transform of the full THz pulse containing all transients from internal reflections from the measurement of graphene-covered substrate. The distance between peaks in frequency domain ($f_p$) in the Fourier transformed signal depends on $d_{sub}$ ($d_{sub} = c/(n_{sub}f_p)$). We generally determine the thickness of nominally $525 \pm 5\,\mu m$ Si wafers as $524.2 \pm 0.2\,\mu m$ for the samples studied here. Thickness determination from THz-TDS is a subject of much work itself [33,34]. In the present study we are able to reliably determine the thickness $d_{sub}$ from graphene-covered substrate, but we note that the thickness determination may become less straight-forward for thin films that are not of single-atomic thickness.

First, we describe how to implement the reference-free methodology with THz-TDS data obtained from the custom-built ultra-broadband setup. Compared to the commercial setup, the custom-built setup not only offers better accuracy of the Drude model fits for electrical property determination due to much broader frequency range; the extremely short pulse duration (few tens of fs, see Fig. 1) also enables measurements on very thin sample substrates with which commercial setups usually end up with un-separable echo transients [6,27]. When the THz frequency increases, the silicon absorption becomes more noticeable and cannot be ignored [32,35] and frequency-dependent THz wave attenuation has also been reported when multiple high-resistivity Si plates were used as broadband THz attenuators [36]. Practically, with one single scan on bare substrate, the ratio $T = |\tilde{E}_{sub}^{(1st)}/\tilde{E}_{sub}^{(dir)}|$ between the first echo and directly transmitted transients will count for all substrate relevant THz wave attenuation and give the amplitude correction term when comparing to $(n_{sub} - 1)^2/(n_{sub} + 1)^2$.

The graphene conductivity retrieval from the reference-free analysis ($\tilde{\sigma}_s^{(ref\text{-}free)}(\omega)$) is shown together with the results from the standard referenced analysis ($\tilde{\sigma}_s^{(1st)}(\omega)$) based on the same THz-TDS sample measurement in Fig. 2. When the amplitude correction is not included, the

real part of the conductivity of $\tilde{\sigma}_s^{(\text{ref-free})}(\omega)$ shows an artificially higher value in the high frequency range. This can be easily understood; without correction, the frequency-dependent substrate material induced loss is simply counted as graphene absorption, and thus leads to higher conductivity. The Gouy phase correction does not make significant change in this case. The relatively loose focus condition for the incident THz beam into the sample and high frequency range in the setup could be the explanation. In practice, the Gouy phase correction is implemented by taking the phase shift $\Delta\emptyset_{\text{sub}}$ between the first echo and direct transmission signals in a single bare substrate waveform scan, since $e^{-2i\omega d_{\text{sub}}n_{\text{sub}}/c}e^{-i\emptyset_G} = e^{-i\Delta\emptyset_{\text{sub}}}$. It is clear that the results obtained from the reference-free analysis including Gouy phase and amplitude corrections are very similar to the results from the standard referenced analysis across a broad frequency range, except that the imaginary part for the reference-free analysis appears more oscillatory.
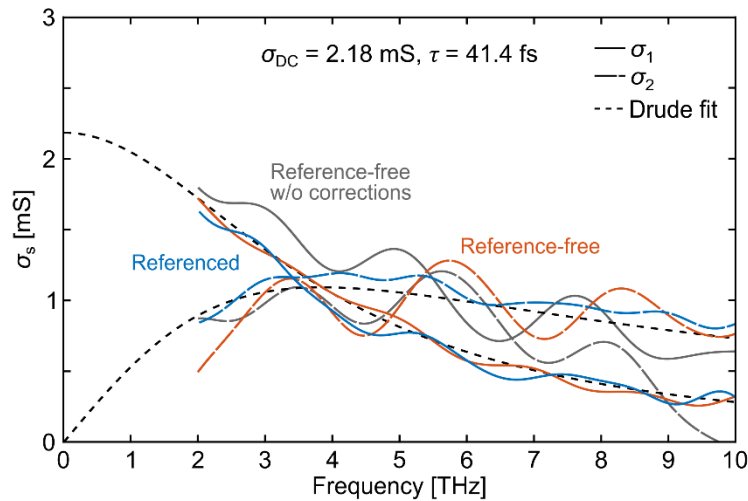


**Fig. 2.** Sheet conductivity spectra for graphene together with a fit to the Drude model. Data is acquired with custom-built broadband THz spectrometer.

Even though we here obtain the amplitude and Gouy phase corrections needed for improving the accuracy of the measured $\tilde{\sigma}_s^{(\text{ref-free})}(\omega)$ by running one scan through bare substrate material, it is worth to mention that these steps are a one-off procedure for calibration of the instrument and its response. It is therefore very different from the standard referenced analysis. The amplitude correction term is solely dependent on the substrate material absorption, while the Gouy phase shift correction is caused by the THz focusing geometry and sample thickness. Therefore, the abovementioned corrections, if needed, only require one single calibration-like measurement that can be taken at a very different time. In contrast, in standard referenced analysis, the reference scans need to be frequently taken and paired up with the sample measurements, since it is sensitive to all sorts of fluctuations from THz source, environment, mechanical movement, etc.

For the narrow-band measurements with the commercial setup the absorption loss related amplitude correction term can be ignored, since high-resistivity Si has a negligible absorption in the low frequency range [32]. We need to investigate the Gouy phase correction since the presence of this is more likely to influence measurements for a tightly focused low-frequency THz wave [31].

Figure 3 shows a comparison of $\tilde{\sigma}_s(\omega)$ extracted from standard referenced and reference-free analysis based on the same THz-TDS sample measurement using the commercial setup. The

results from fits with the Drude model are similar for both $\sigma_{DC}$ and $\tau$ for standard referenced and reference-free analysis, which shows that the reference-free analysis also works at lower THz frequencies.
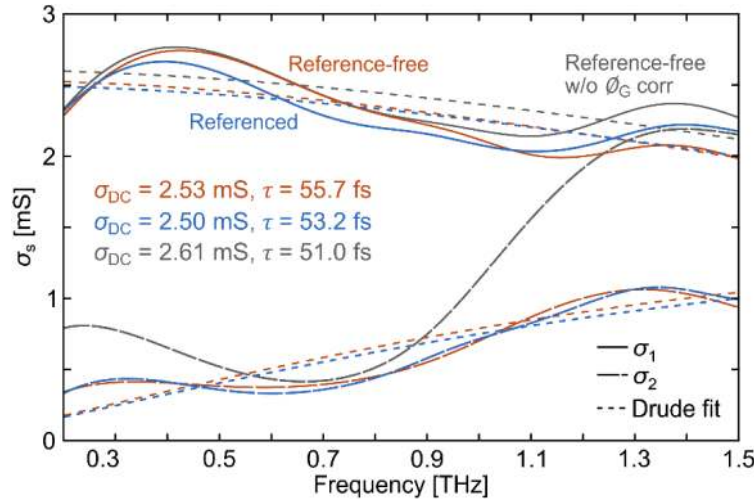


**Fig. 3.** Sheet conductivity spectra for graphene together with fits to the Drude model. Data is acquired with the commercial THz-TDS setup.

We also show the results from a reference-free analysis without the Gouy shift phase term in Fig. 3. Here, it is observed that the imaginary part of $\tilde{\sigma}_s(\omega)$ oscillates more drastically as expected when measuring with a tightly focused low-frequency THz wave [31], and an attempt to fit this dataset with the Drude model appears meaningless. However, the effect on the real part of $\tilde{\sigma}_s^{(ref-free)}(\omega)$ is less significant in the case where the Gouy phase shift is not included. We therefore only fit the real part of $\tilde{\sigma}_s(\omega)$ to the Drude model in this case and actually find that the results for both $\sigma_{DC}$ and $\tau$ are still in relatively good agreement (~5%) when compared to the referenced measurement. We highlight here that the reference-free method without $\emptyset_G$ correction does not require any scan of a reference substrate and is therefore in fact independent of the instrument calibration procedure.

In order to obtain some statistical information, we performed a THz-TDS map of a sample (~$10 \times 10$ mm$^2$) with 200-µm step size with the commercial setup. Figure 4(a) shows an optical map acquired with an optical microscope of the graphene sample used for THz-TDS mapping of the electrical properties of graphene. The sample has some features that should be clearly visible in the THz-TDS maps of electrical properties like the large tear in the top of the sample. Such irregular features are deemed of particular interest for a comparison of different methods for mapping techniques to highlight similarities (or lack of such) between methods. The graphene coverage map (Fig. 4(b)) calculated from the optical map shows that all the graphene present is single layer and that the sample contains more defects in the upper half of it. A high magnification optical image (Fig. 4(c)) confirms that the graphene is in general continuous with some smaller tears that are insignificant for a THz-TDS measurement spot size of hundreds of µm [2,14,37].

Figures 4(d)-(f) compares THz-TDS maps of $\sigma_{DC}$ based on standard referenced analysis, reference-free analysis and reference-free analysis without $\emptyset_G$ correction for the sample. The maps clearly highlight the same trends – they both show the "large" hole in the top of the graphene sheet, a region of slightly lower conductivity towards the top left and a higher conductivity towards the bottom. The main difference is found for the reference-free analysis without $\emptyset_G$
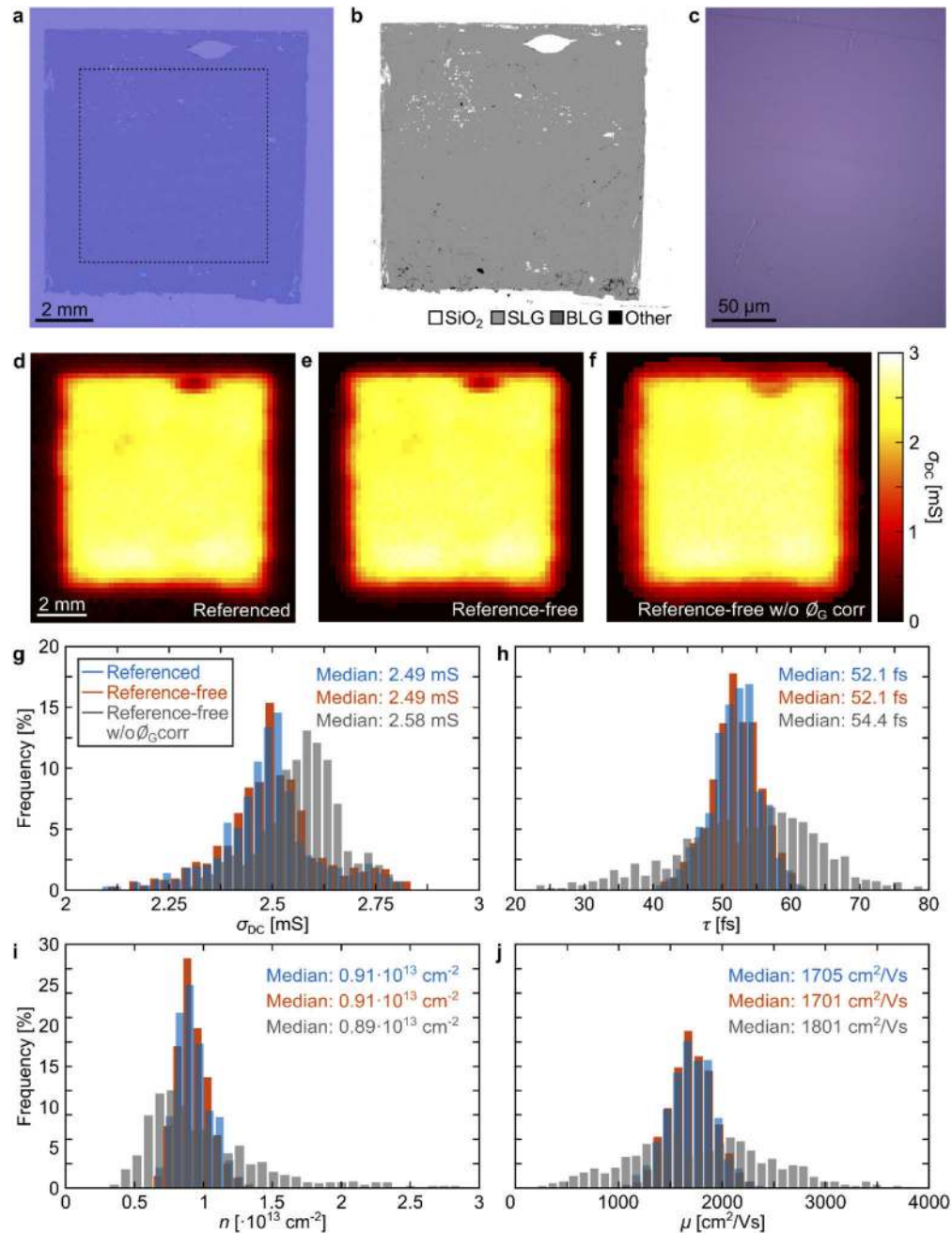
**Fig. 4.** (a) Optical map of graphene on 90 nm SiO2/Si substrate. (b) Graphene coverage map of the sample shown in (a). (c) High magnification image from sample shown in (a). Brightness and contrast has been increased for (a,c) for clarity. (d-f) THz-TDS DC sheet conductivity maps of graphene sample shown in (a) based on (d) standard referenced analysis, (e) reference-free analysis and (f) reference-free analysis without Gouy phase correction. (g-j) Histograms with comparisons of electrical parameters extracted from reference-free and standard referenced analysis. (g) DC conductivity. (h) Scattering time. (i) Carrier density. (j) Mobility. Values for histograms are taken within the dotted square in (a).

correction at the edges of the graphene covered region of the sample where the values for $\sigma_{DC}$ fades slower towards 0 mS and the region of slightly lower conductivity is perhaps less obvious.

In general, the two $\sigma_{DC}$ maps for standard referenced analysis and reference-free analysis in Figs. 4(d),(e) are in very good agreement. This is further highlighted by the histogram in Fig. 4 g of the $\sigma_{DC}$ values from the two maps, where the median $\sigma_{DC}$ value for both agree at 2.49 mS and the spread in the histograms is similar. Histograms of $\tau$, $n$ and $\mu$ are shown in Figs. 4(h)-(j) and for $v_F^*$ in Fig. 5 and all show excellent agreement between data obtained from standard referenced analysis and reference-free analysis.
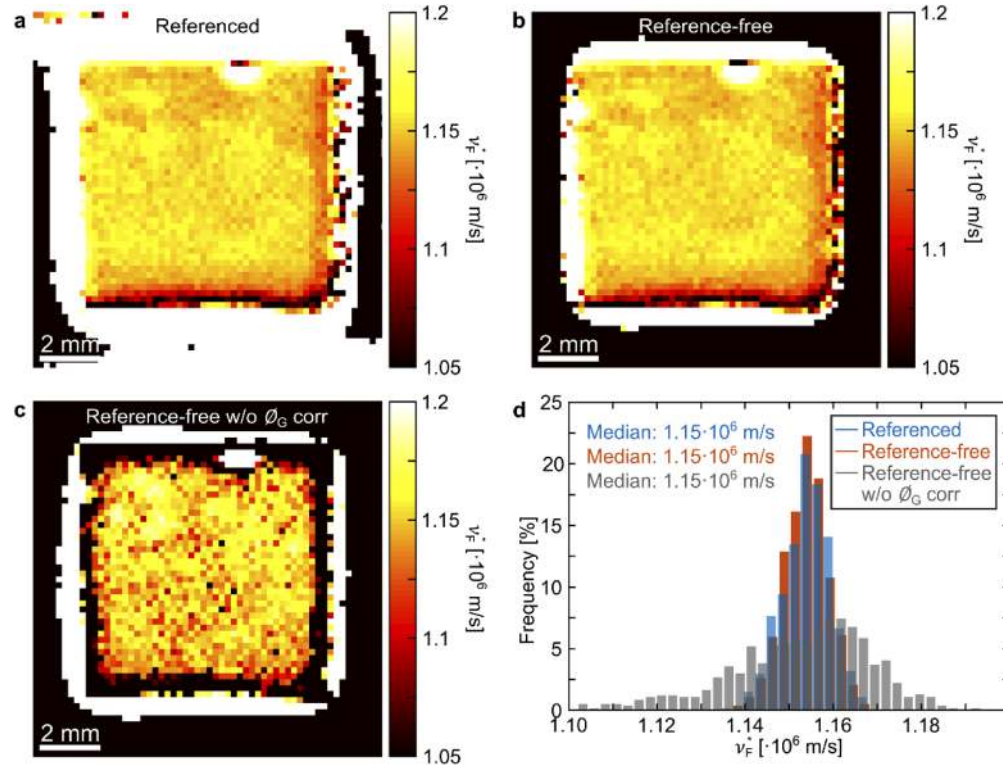


**Fig. 5.** (a-c) THz-TDS maps of renormalized Fermi velocity for the sample shown in Fig. 4 based on (a) standard referenced analysis, (b) reference-free analysis and (c) reference-free analysis without Gouy phase correction. (d) Histogram of $v_F^*$ values from maps in (a-c).

For the reference-free analysis without $\emptyset_G$ correction the median values agree reasonably well (within 5%) when compared to the standard referenced analysis (Figs. 4(g)-(j)). There is however a clear offset in the values for $\sigma_{DC}$, while there is a much larger spread for $\tau$. Since $n$ and $\mu$ depends on the square of $\tau$ (Eqs. (4) and 5) we also here see that the spread is larger for the reference-free analysis. The same trend for the spread is seen for $v_F^*$ in Fig. 5 although there the median values agree perfectly at $1.15 \cdot 10^6$ m/s. Interestingly, the maps of $v_F^*$ in Fig. 5 show a structure that is similar to the $\sigma_{DC}$ maps in Fig. 4, but with some even clearer variations across the sample that follows the areas with smaller holes and tears in the graphene coverage map in Fig. 4(b). The larger spread for the reference-free analysis without $\emptyset_G$ correction is also clearly observed in the map of $v_F^*$ in Fig. 5(c).

Depending on the required measurement accuracy it is thus possible to measure and map the conductivity of thin conducting films from THz-TDS measurements without the need of any reference measurements which greatly improves the ease of measuring, especially for substrates

that are fully covered by conducting film where a separate reference sample is required. If greater accuracy is required this method with inclusion of amplitude and Gouy phase shift correction terms still holds clear benefits compared to standard reference analysis regarding robustness. We note that the reference-free analysis is limited to cases where the time-domain THz transients from internal reflection are well-separated in time. This is fine for most modern THz-TDS setups when measuring on standard wafer-based substrates with thicknesses above several hundreds of µm and relatively high $n_{sub}$. For thin polymeric substrates with low $n_{sub}$ (often $n_{sub} < 2$) there is a requirement for development of THz-TDS setups with short pulse durations (like the air plasma setups used here) capable of rapidly acquiring data from many measurement points.

## 4. Conclusion

In conclusion, we have presented a reference-free THz-TDS technique to determine the electrical properties of graphene. By using THz transients originating from internal reflections in the graphene covered substrate we experimentally demonstrate extraction of the electrical properties of graphene from a single THz time-domain waveform without the need for a reference scan. We identify two important terms that influence retrieval deviations and discuss simple and robust correction methods for higher retrieval accuracy. Excellent agreement was obtained between the reference-free analysis and the standard referenced analysis in two different THz-TDS systems and across an extended frequency range. Furthermore, with the reference-free technique, we also demonstrate spatial mapping of a wide range of electrical parameters of graphene, such as DC sheet conductivity $\sigma_{DC}$, scattering time $\tau$, carrier density $n$, mobility $\mu$, and renormalized Fermi velocity $v_F^*$. This technique is generally applicable for electrical property analysis of thin conducting films.

## Funding

## Disclosures

The authors declare no conflicts of interest.

## References

1. I. Ivanov, M. Bonn, Z. Mics, and D. Turchinovich, "Perspective on terahertz spectroscopy of graphene," Europhys. Lett. **111**(6), 67001 (2015).
2. P. Bøggild, D. M. A. Mackenzie, P. R. Whelan, D. H. Petersen, J. D. Buron, A. Zurutuza, J. Gallop, L. Hao, and P. U. Jepsen, "Mapping the electrical properties of large-area graphene," 2D Mater. **4**(4), 042003 (2017).
3. P. Kužel and H. Němec, "Terahertz Spectroscopy of Nanomaterials: a Close Look at Charge-Carrier Transport," Adv. Opt. Mater. **8**(3), 1900623 (2020).
4. H. A. Hafez, S. K. Klaas, K. J. Tielrooij, M. Bonn, M. Gensch, and D. Turchinovich, "Terahertz Nonlinear Optics of Graphene: From Saturable Absorption to High-Harmonics Generation," Adv. Opt. Mater. **8**(3), 1900771 (2020).
5. C. Melios, N. Huang, L. Callegaro, A. Centeno, A. Cultrera, A. Cordon, V. Panchal, I. Arnedo, A. Redo-Sanchez, D. Etayo, M. Fernandez, A. Lopez, S. Rozhko, O. Txoperena, A. Zurutuza, and O. Kazakova, "Towards standardisation of contact and contactless electrical measurements of CVD graphene at the macro-, micro- and nano-scale," Sci. Rep. **10**(1), 3223 (2020).
6. P. R. Whelan, D. P. Huang, D. Mackenzie, S. A. Messina, Z. C. Li, X. Li, Y. Q. Li, T. J. Booth, P. U. Jepsen, H. F. Shi, and P. Bøggild, "Conductivity mapping of graphene on polymeric films by terahertz time-domain spectroscopy," Opt. Express **26**(14), 17748–17754 (2018).
7. A. Rehn, D. Jahn, J. C. Balzer, and M. Koch, "Periodic sampling errors in terahertz time-domain measurements," Opt. Express **25**(6), 6712–6724 (2017).
8. P. R. Whelan, K. Iwaszczuk, R. Z. Wang, S. Hofmann, P. Bøggild, and P. U. Jepsen, "Robust mapping of electrical properties of graphene from terahertz time-domain spectroscopy with timing jitter correction," Opt. Express **25**(3), 2725–2732 (2017).
9. H. Němec, F. Kadlec, P. Kužel, L. Duvillaret, and J. L. Coutaz, "Independent determination of the complex refractive index and wave impedance by time-domain terahertz spectroscopy," Opt. Commun. **260**(1), 175–183 (2006).

10. P. U. Jepsen, U. Møller, and H. Merbold, "Invesigation of aqueous alcohol and sugar solutions with reflection terahertz time-domain spectroscopy," Opt. Express **15**(22), 14717–14737 (2007).

11. E. A. Ladron, M. Chudzik, A. L. Zorzano, D. E. Salinas, L. E. H. Arroyo, and A. Z. Elorza, "Quality inspection of thin film materials," U.S. Patent 2018164354 (2018).

12. H. Y. Lin, O. J. Burton, S. Engelbrecht, K. Tybussek, B. M. Fischer, and S. Hofmann, "Through-substrate terahertz time-domain reflection spectroscopy for environmental graphene conductivity mapping," Appl. Phys. Lett. **116**(2), 021105 (2020).

13. J. L. Tomaino, A. D. Jameson, J. W. Kevek, M. J. Paul, A. M. van der Zande, R. A. Barton, P. L. McEuen, E. D. Minot, and Y. S. Lee, "Terahertz imaging and spectroscopy of large-area single-layer graphene," Opt. Express **19**(1), 141–146 (2011).

14. J. D. Buron, D. H. Petersen, P. Bøggild, D. G. Cooke, M. Hilke, J. Sun, E. Whiteway, P. F. Nielsen, O. Hansen, A. Yurgens, and P. U. Jepsen, "Graphene conductance uniformity mapping," Nano Lett. **12**(10), 5074–5081 (2012).

15. J. Gorecki, N. Klokkou, L. Piper, S. Mailis, N. Papasimakis, and V. Apostolopoulos, "High precision THz-TDS via self-referenced transmission echo method," Appl. Opt. **59**(22), 6744–6750 (2020).

16. D. Luo, M. H. Wang, Y. Q. Li, C. Kim, K. M. Yu, Y. Kim, H. J. Han, M. Biswal, M. Huang, Y. Kwon, M. Goo, D. C. Camachomojica, H. F. Shi, W. J. Yoo, M. S. Altman, H. Shin, and R. S. Ruoff, "Adlayer-Free Large-Area Single Crystal Graphene Grown on a Cu(111) Foil," Adv. Mater. **31**(35), 1903615 (2019).

17. S. Jin, M. Huang, Y. Kwon, L. Zhang, B. W. Li, S. Oh, J. Dong, D. Luo, M. Biswal, B. V. Cunning, P. V. Bakharev, I. Moon, W. J. Yoo, D. C. Camachomojica, Y. Kim, S. H. Lee, B. Wang, W. K. Seong, M. Saxena, F. Ding, H. Shin, and R. S. Ruoff, "Colossal grain growth yields single-crystal metal foils by contact-free annealing," Science **362**(6418), 1021–1025 (2018).

18. M. Huang, M. Biswal, H. J. Park, S. Jin, D. Qu, S. Hong, Z. Zhu, L. Qiu, D. Luo, X. C. Liu, Z. Yang, Z. L. Liu, Y. Huang, H. Lim, W. J. Yoo, F. Ding, Y. L. Wang, Z. Lee, and R. S. Ruoff, "Highly Oriented Monolayer Graphene Grown on a Cu/Ni(111) Alloy Foil," ACS Nano **12**(6), 6117–6127 (2018).

19. B. S. Jessen, P. R. Whelan, D. M. A. Mackenzie, B. R. Luo, J. D. Thomsen, L. Gammelgaard, T. Booth, and P. Bøggild, "Quantitative optical mapping of two-dimensional materials," Sci. Rep. **8**(1), 6381 (2018).

20. A. T. Tarekegne, B. B. Zhou, K. J. Kaltenecker, K. Iwaszczuk, S. J. Clark, and P. U. Jepsen, "Terahertz time-domain spectroscopy of zone-folded acoustic phonons in 4H and 6H silicon carbide," Opt. Express **27**(3), 3618–3628 (2019).

21. J. Dai, X. Xie, and X. C. Zhang, "Detection of Broadband Terahertz Waves with a Laser-Induced Plasma in Gases," Phys. Rev. Lett. **97**(10), 103903 (2006).

22. T. Wang, K. Iwaszczuk, E. A. Wrisberg, E. V. Denning, and P. U. Jepsen, "Linearity of Air-Biased Coherent Detection for Terahertz Time-Domain Spectroscopy," J. Infrared, Millimeter, Terahertz Waves **37**(6), 592–604 (2016).

23. R. E. Glover and M. Tinkham, "Conductivity of Superconducting Films for Photon Energies between 0.3 and 40 kTc," Phys. Rev. **108**(2), 243–256 (1957).

24. J. D. Buron, D. M. A. Mackenzie, D. H. Petersen, A. Pesquera, A. Centeno, P. Bøggild, A. Zurutuza, and P. U. Jepsen, "Terahertz wafer-scale mobility mapping of graphene on insulating substrates without a gate," Opt. Express **23**(24), 30721–30729 (2015).

25. P. R. Whelan, X. J. Zhao, I. Pasternak, W. Strupinski, P. U. Jepsen, and P. Bøggild, "Non-contact mobility measurements of graphene on silicon carbide," Microelectron. Eng. **212**, 9–12 (2019).

26. T. Stauber, N. M. R. Peres, and A. H. Castro-Neto, "Conductivity of suspended and non-suspended graphene at finite gate voltage," Phys. Rev. B **78**(8), 085418 (2008).

27. P. R. Whelan, Q. Shen, B. B. Zhou, I. G. Serrano, M. V. Kamalakar, D. M. A. Mackenzie, J. Ji, D. P. Huang, H. F. Shi, D. Luo, M. H. Wang, R. S. Ruoff, A. Jauho, P. U. Jepsen, P. Bøggild, and J. M. Caridad, "Fermi velocity renormalization in graphene probed by terahertz time-domain spectroscopy," 2D Mater. **7**(3), 035009 (2020).

28. J. González, F. Guinea, and M. A. H. Vozmediano, "Non-Fermi liquid behavior of electrons in the half-filled honeycomb lattice (A renormalization group approach)," Nucl. Phys. B **424**(3), 595–618 (1994).

29. S. D. Sarma, E. H. Hwang, and W. K. Tse, "Many-body interaction effects in doped and undoped graphene: Fermi liquid versus non-Fermi liquid," Phys. Rev. B **75**(12), 121406 (2007).

30. T. Stauber, P. Parida, M. Trushin, M. V. Ulybyshev, D. L. Boyda, and J. Schliemann, "Interacting Electrons in Graphene: Fermi Velocity Renormalization and Optical Response," Phys. Rev. Lett. **118**(26), 266801 (2017).

31. P. Kužel, H. Němec, F. Kadlec, and C. Kadlec, "Gouy shift correction for highly accurate refractive index retrieval in time-domain terahertz spectroscopy," Opt. Express **18**(15), 15338–15348 (2010).

32. J. Dai, J. Zhang, W. Zhang, and D. Grischkowsky, "Terahertz time-domain spectroscopy characterization of the far-infrared absorption and index of refraction of high-resistivity, float-zone silicon," J. Opt. Soc. Am. B **21**(7), 1379–1386 (2004).

33. C. Kadlec, F. Kadlec, H. Němec, P. Kužel, J. Schubert, and G. Panaitov, "High tunability of the soft mode in strained SrTiO3/DyScO3 multilayers," J. Phys.: Condens. Matter **21**(11), 115902 (2009).

34. K. L. Krewer, Z. Mics, J. Arabski, G. Schmerber, E. Beaurepaire, M. Bonn, and D. Turchinovich, "Accurate terahertz spectroscopy of supported thin films by precise substrate thickness correction," Opt. Lett. **43**(3), 447–450 (2018).

35. B. B. Zhou, Q. Shen, and P. U. Jepsen, "Ultra-broadband characterization of high-resistivity silicon by 2-color air-plasma terahertz time-domain spectroscopy," *In preparation* (2020).

36. K. J. Kaltenecker, E. J. R. Kelleher, B. B. Zhou, and P. U. Jepsen, "Attenuation of THz beams: a 'how to' tutorial," J. Infrared, Millimeter, Terahertz Waves **40**(8), 878–904 (2019).

37. P. R. Whelan, V. Panchal, D. H. Petersen, D. M. A. Mackenzie, C. Melios, I. Pasternak, J. C. Gallop, F. W. Osterberg, P. U. Jepsen, W. Strupinski, O. Kazakova, and P. Bøggild, "Electrical Homogeneity Mapping of Epitaxial Graphene on Silicon Carbide," ACS Appl. Mater. Interfaces **10**(37), 31641–31647 (2018).